Impact of Labrador Sea Convection on the North Atlantic Meridional Overturning Circulation

ROBERT S. PICKART AND MICHAEL A. SPALL

Woods Hole Oceanographic Institution, Woods Hole, Massachusetts

(Manuscript received 18 September 2005, in final form 21 May 2007)

ABSTRACT

The overturning and horizontal circulations of the Labrador Sea are deduced from a composite vertical section across the basin. The data come from the late-spring/early-summer occupations of the World Ocean Circulation Experiment (WOCE) AR7W line, during the years 1990–97. This time period was chosen because it corresponded to intense wintertime convection—the deepest and densest in the historical record—suggesting that the North Atlantic meridional overturning circulation (MOC) would be maximally impacted. The composite geostrophic velocity section was referenced using a mean lateral velocity profile from float data and then subsequently adjusted to balance mass. The analysis was done in depth space to determine the net sinking that results from convection and in density space to determine the diapycnal mass flux (i.e., the transformation of light water to Labrador Sea Water). The mean overturning cell is calculated to be 1 Sv (1 Sv $\equiv 10^6$ m^3 s^{-1}), as compared with a horizontal gyre of 18 Sv. The total water mass transformation is 2 Sv. These values are consistent with recent modeling results. The diagnosed heat flux of 37.6 TW is found to result predominantly from the horizontal circulation, both in depth space and density space. These results suggest that the North Atlantic MOC is not largely impacted by deep convection in the Labrador Sea.

1. Introduction

Much has been made of the role of the ocean's meridional overturning circulation (MOC), and the heat that it transports, in dictating global climate. For example, inferred changes in the strength of the overturning have been linked with significant shifts in sea surface and air temperatures in the paleoclimate record (McManus et al. 2004). Such changes in MOC strength are believed to be at the heart of the climate system's response to future greenhouse warming scenarios (e.g., Stocker and Schmittner 1997; Rahmstorf 1997; Clark et al. 2002). In the North Atlantic Ocean, warm surface waters flux more than a petawatt of heat northward at 24°N (Hall and Bryden 1982), which is then released to the atmosphere at high latitudes during the process of densification and convective overturning. The intermediate and deep-water masses so formed then flow equatorward to complete the MOC cell. Typical estimates of the strength of the North Atlantic overturning cell are in the range of 13–15 Sv (1 Sv $\equiv 10^6$ m^3 s^{-1}; e.g., Schmitz and McCartney 1993).

The two main regions of deep convection, and the most significant densification in the North Atlantic in terms of the MOC, are the Nordic seas and the Labrador/Irminger Seas. The former is the source of North Atlantic Deep Water (e.g., Swift 1984; Mauritzen 1996), which occupies the bottom-most layer in the subpolar North Atlantic, and the latter is the location where the middepth water mass known as Labrador Sea Water (LSW) is formed (e.g., Clarke and Gascard 1983; Pickart et al. 2003a). While it is clear that the sinking associated with the formation of North Atlantic Deep Water—for example, the cascading of dense water downstream of Denmark Strait—is a major component of the MOC, the contribution to the MOC from the formation of LSW is less certain.

A commonly used method of quantifying sinking is the use of zonally averaged overturning streamfunctions. Some of the published overturning cells from numerical models show a large amount of sinking at middepth, particularly in low-resolution climate models. For example, Delworth et al.'s (1993) model shows 6–7

Corresponding author address: Robert S. Pickart, Department of Physical Oceanography, Woods Hole Oceanographic Institution, MS 21, Woods Hole, MA 02543.
E-mail: rpickart@whoi.edu

DOI: 10.1175/JPO3178.1

Sv of overturning in the upper 2 km of the water column. Talley et al. (2003) present an overturning streamfunction derived from historical data, which has a middepth contribution of similar magnitude. Results such as these give the impression that the Labrador Sea plays a major role in the MOC. However, climate models are not sufficient to depict the details of the circulation and convection in the Labrador Sea, and it is often unclear where the sinking takes place longitudinally in such simulations.

Part of the uncertainty regarding the Labrador Sea's contribution to the MOC centers around the concept of water mass transformation versus Eulerian sinking of water. Convective mixing occurs frequently during wintertime in the Labrador Sea, and as a result the LSW mode water is formed (e.g., Lazier et al. 2002). However, such ventilation and water mass transformation does not necessarily imply net sinking of water. In fact, Spall and Pickart (2001) showed that a significant vertical volume flux in midbasin at high latitudes would have to be accompanied by a very large horizontal circulation. They argued that even a small amount of interior downwelling in the Labrador Sea (or any other interior basin) is therefore unlikely.

In the numerical simulations of Spall and Pickart (2001) sinking did occur in the subpolar North Atlantic, but it occurred near the lateral boundaries of the model above the continental slope. This was true in Spall's (2004) eddy-resolving idealized model of a marginal sea as well. A simple analytical estimate of the boundary sinking was derived by Spall and Pickart (2001) that depends on the lateral gradient of density along the boundary. Applying this estimate to the Labrador Sea, using sparse wintertime data, they obtained a sinking estimate of only 1 Sv. This may seem at odds with some of the climate models, although it is consistent with the numerical results of Böning et al. (1996), who did a series of high-resolution model runs to investigate the nature of the North Atlantic MOC. They found that most of the sinking occurred near topographic boundaries, and that deep convection in the Labrador Sea contributed very little to the overall transport of the MOC. This was a robust feature over the range of parameters considered, and in the highest-resolution simulation (1/6°) the sinking in the Labrador Sea was 1.3 Sv, in line with Spall and Pickart's (2001) estimate.

The Labrador Sea's contribution to the MOC in terms of diapycnal mass flux, as opposed to Eulerian sinking, is equally uncertain at this point. There are numerous estimates of transformation using different approaches, including local observations in the Labrador Sea, air–sea flux calculations, regional tracer budgets, and ocean basin box models. Estimates of LSW formation rates range greatly, from 1 to 10 Sv (see Table 1). It should be noted that a few of these values are based on the assumption that nearly all of the newly ventilated LSW drains away from the basin each year. This is clearly not the case (see Lazier et al. 2002), and it is unknown what percentage is fluxed laterally out of the Labrador Sea during summer and fall. Some of the variation in the transformation rates in Table 1 could be due to temporal variability, as the various studies span several decades. Using chlorofluorocarbon (CFC) inventories, Rhein et al. (2002) argued that during the period of intense convection in the Labrador Sea in the early 1990s the transformation increased significantly to more than 10 Sv. This is consistent with the results of Marsh (2000), who used buoyancy fluxes to deduce a time series of LSW transformation.

TABLE 1. Data-based Labrador Sea Water formation rates from the literature.

Study	Formation rate (Sv)	Method
Wright (1972)	3.5	Inferred from air–sea fluxes
Worthington (1976)	2	Box model
Clarke and Gascard (1983)	3.9	Wintertime observations
McCartney and Talley (1984)	8.5	Box model
McCartney (1992)	2	Mass budget
Speer et al. (1995)	1	Inferred from air–sea fluxes
Marsh (2000)	3.4	Inferred from air–sea fluxes
Smethie and Fine (2001)	7.4	Tracer inventory
Rhein et al. (2002)	4.4–5.6	Tracer inventory
Talley (2003)	7	Inverse calculation
	Average: 4.4 ± 2.4	

Using the large-scale velocity dataset of Reid (1994), Talley (2003) and Talley et al. (2003) constructed an overturning streamfunction in density space for the Atlantic Ocean in which the LSW overturning cell is 7 Sv. It should be noted, however, that the northernmost hydrographic section used in their calculation is situated at 59.5°N, which is farther north than the region of strong heat loss and deep convection in the Labrador Sea. Hence the overturning of 7 Sv evidently applies to the formation of subpolar mode water outside of the Labrador Sea in the eastern Atlantic. Models have also provided estimates of the diapycnal mass flux associated with formation of LSW. Böning et al.'s (1996) numerical simulations suggest roughly 5 Sv of transformation, Brandt et al. (2007) have 6–7 Sv of LSW formation, and Mauritzen and Häkkinen (1999) have 8–9 Sv.

Straneo's (2006) analytical model of a boundary current encircling an interior convective basin gives only 2 Sv when constrained with parameters specific to the Labrador Sea. With regard to interannual variability, the time series of LSW transformation in Marsh et al.'s (2005) eddy-permitting model shows substantial variation over the last 20 yr, with values over 10 Sv for the strong convection period of the early 1990s.

In terms of climate, it is of fundamental importance to understand the mechanisms responsible for the northward transport of heat in the North Atlantic. Hence, one needs to consider not only the MOC, but the vertically averaged circulation as well, that is, the horizontal gyres. Using a trans-Atlantic hydrographic section at 24°N, together with current meter data in the Florida Straits, Hall and Bryden (1982) determined that the dominant component of the poleward heat flux was in fact due to the barotropic circulation.[1] In the model study of Böning et al. (1996) the horizontal circulation (together with the Ekman contribution) accounted for 25% of the total heat flux. In the subpolar North Atlantic, Spall and Pickart's (2001) numerical simulations suggest that the heat flux at high latitudes is predominantly due to the horizontal gyre circulation. This is consistent with Spall's (2004) marginal sea model where the horizontal heat flux is much greater than the overturning heat flux. Note that all of these studies were carried out in a depth framework. Talley (2003) diagnosed the North Atlantic heat flux in density space and found that the overturning circulation in this framework was associated with a significant heat flux. Talley (2003) considered separately the shallow, intermediate, and deep components of the overturning cell, and found that the middepth component, in the density range of the LSW, accounted for a third of the total heat flux.

In this paper we use hydrographic and Lagrangian float data to diagnose the horizontal and overturning circulation in the Labrador Sea, and the corresponding heat flux. The overall goal is to clarify some of the uncertainties noted above regarding the contribution of the Labrador Sea to the North Atlantic MOC. Two important aspects of the dataset are that the hydrographic section across the basin is a composite of 10 occupations, and the float data, also averaged in time, enable the computation of absolute geostrophic velocities. This results in reduced errors and removes ambiguities and assumptions that arise from the use of nonreferenced velocities. By working in both depth space and density space, we distinguish explicitly between downwelling and diapycnal mass flux, that is sinking versus transformation. We also partition the heat flux into its contribution due to the overturning cell versus the horizontal gyre circulation. Last, the observational results are interpreted in the context of a recent model study.

[1] Hall and Bryden (1982) did discuss an alternative interpretation of their data that increased the importance of the overturning component, but this aspect of the analysis was not quantitative.

2. Mean hydrography

In 1990 the Bedford Institute of Oceanography (BIO) began a program of repeat hydrographic sections across the central Labrador Sea as part of the World Ocean Circulation Experiment (WOCE). The yearly section, known as the AR7W line, is typically done in late spring/early summer and extends from the Labrador shelf to the West Greenland shelf (Fig. 1). The time series has continued beyond WOCE and is still ongoing; occasionally an extra section is occupied during one of the other seasons. Here we consider the 10 nonwinter occupations of AR7W from 1990 to 1997 (Fig. 1). We chose this subset because it encompasses the time period of intense deep convection in the Labrador Sea associated with the well-known high phase of the North Atlantic Oscillation (NAO) during the late 1980s to early 1990s (Dickson et al. 1996). Convection during this period reached a record depth of more than 2 km and produced the densest LSW in the historical record (Lazier et al. 2002). We reason, therefore, that if the North Atlantic MOC is significantly impacted by overturning in the Labrador Sea, this would be the ideal time period to document it. With regard to the seasonal timing of the AR7W occupation, one might argue that late spring is a good time of year to capture the meridional overturning circulation resulting from the recently completed convection. The model results in section 6, as well as those in Straneo's (2006) model, suggest that the maximum seasonal outflow of newly formed LSW occurs in June/July. Brandt et al.'s (2007) simulation has the outflow peak earlier than this; while in June, it is close to the annual mean. We include the two fall occupations in our collection of sections to reduce further the error in the mean velocity section (see below).

The processed conductivity–temperature–depth (CTD) data were obtained from BIO (except for the fall 1994 occupation, which was provided by the Center of Marine and Climate Research, Hamburg, Germany). The 1992 section was terminated halfway across the basin, and the fall 1994 section contained a gap in the middle; otherwise the sections were complete. Typical station spacing was 20–30 km near the western boundary, 55 km in the interior, and 10–30 km near the eastern boundary. For each occupation the data were grid-

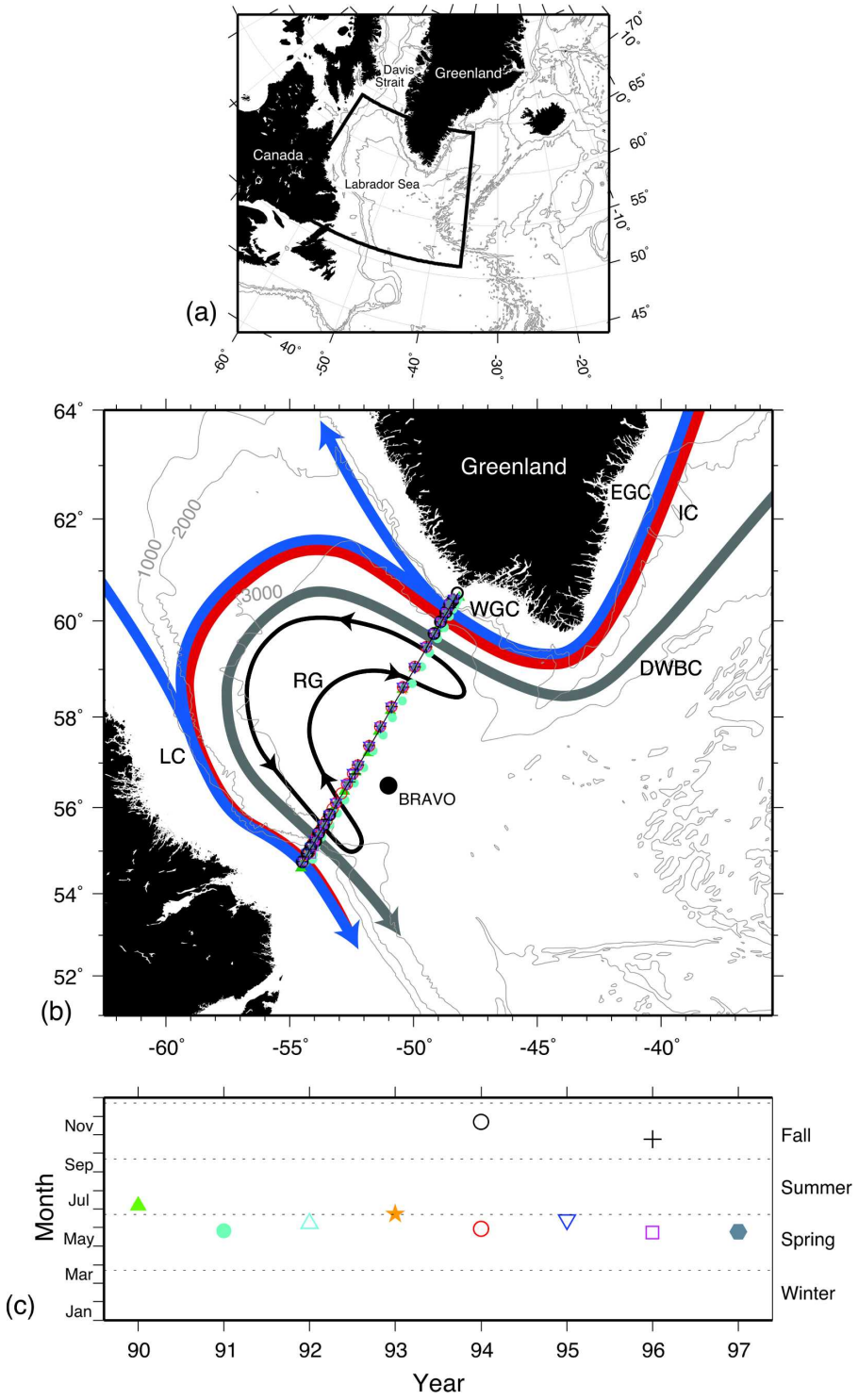

FIG. 1. (a) Study area of the Labrador Sea in the larger context of the western North Atlantic. (b) Schematic circulation in the Labrador Sea. Red (blue) indicates a warm (cold) upper-layer current. East of Greenland the warm, salty Irminger Current (IC) flows alongside the cold, fresh East Greenland Current (EGC). After rounding the southern tip of Greenland this merged current system is called the West Greenland Current (WGC), part of which crosses the basin to join the cold, fresh outflow from Davis Strait to become the Labrador Current (LC). The decreasing amount of red color in the schematic indicates that the presence of the warm Irminger water diminishes significantly in the western Labrador Sea. The gray line denotes the Deep Western Boundary Current (DWBC), and the thin black line indicates the cyclonic recirculation gyre (RG) in the central basin. The stations making up the AR7W hydrographic line are indicated by the discrete symbols, overlaid on the regression line used to grid the sections. Ocean Weather Station Bravo is indicated by the black circle. (c) Temporal distribution of the AR7W sections used in the study.

ded in depth space along the regression line in Fig. 1, using a Laplacian-spline interpolation scheme. The grid spacing was 10 km in the horizontal and 25 m in the vertical. For details of this process and information on the individual cruises, the reader is referred to Pickart et al. (2003b). Vertical sections were constructed on this standard grid for different variables, including potential temperature (θ), salinity (S), and potential density referenced to the sea surface (σ_θ). The origin of the sections is on the Labrador shelf, with distance x increasing to the northeast, and the depth coordinate z increases upward. For the analysis in density space we constructed a mean depth–density relationship, which was used to define a scaled depth z' (see Pickart and Smethie 1998 for details). Gridded sections in density space were constructed in analogous fashion with z' as the vertical coordinate (same grid spacing as in the depth framework).

The general circulation of the Labrador Sea consists of a boundary current system encircling the basin and a generally weak interior flow (Fig. 1). On the eastern side of the basin the West Greenland Current transports cold, fresh Arctic origin water along the outer shelf and shelf break, and warm, salty Irminger water along the upper slope. The current bifurcates near 61°N, and the majority of the flow diverts to the western side of the basin and joins the outflow from Davis Strait, forming the Labrador Current. The signature of the Irminger water is reduced on this side of the basin. At the base of the continental slope the Deep Western Boundary Current transports dense overflow water from the Nordic seas. In the interior of the Labrador Basin, the mean flow is characterized by a weaker, nearly depth-independent cyclonic recirculation (Lavender et al. 2000).

The mean hydrographic sections (Fig. 2) depict the state of the Labrador Sea during the period of intense convection during the early to mid-1990s. The newly formed LSW is evident in the middle of the water column as the body of cold, fresh (relative to the boundaries), and weakly stratified water. At this time of year the restratification has begun (e.g., Lilly et al. 1999) and the surface layer is warm from solar heating and fresh from exchange with the low salinity shelfbreak water flowing around the basin. Note the warm and salty Irminger water on the eastern side of the basin centered near 500 m in the West Greenland Current. By the time this water reaches the other side of the basin it is significantly colder and fresher. This modification is due in part to lateral exchange along density surfaces (Cuny et al. 2002), but it is also due to convective overturning in the outer part of the Labrador Current (Pickart et al. 2002). Such boundary convection was observed to reach 1200 m during a wintertime hydrographic survey in 1997.[2] The deep salty layer beneath the LSW is predominantly overflow water from the eastern Atlantic, and the bottommost layer of cold and freshwater is the Denmark Strait Overflow Water. The latter has a higher dissolved oxygen content (not shown).

Although the newly transformed LSW is clearly evident in the mean sections of Fig. 2, in order to quantify this transformation and distinguish it from vertical sinking it is necessary to have the accompanying absolute velocity section.

3. Mean velocity

a. Absolute geostrophic velocity

Using the mean gridded sections of temperature and salinity, an average thermal wind field was constructed. To reference this, we used the directly measured velocity from the Lagrangian float study of Lavender et al. (2000). In that study five years of Profiling Autonomous Lagrangian Circulation Explorer (PALACE) float data, from the time period 1995–99, were averaged together to construct absolute velocity fields at two depth horizons in the western subpolar gyre. We used the data at 700 m along the AR7W line (flow component normal to the section) as the reference to produce a mean vertical section of absolute geostrophic velocity. Most of the float measurements were made after 1995, so in fact there is not much overlap in time between the hydrographic and Lagrangian datasets. Furthermore, as noted above, the extent of deep convection changed after 1997, and other hydrographic changes occurred late in the decade (Lilly et al. 2003). This should be kept in mind when considering the results below. However, the fact that both datasets are multiyear composites is an important advantage in reducing noise that is inherent in synoptic measurements. This includes noise in the density structure (addressed via repeat hydrographic sections) and noise in the barotropic circulation (addressed via multiple years of float data).

As schematized in Fig. 1, in the bottommost layer of the Labrador Sea the Deep Western Boundary Current advects Nordic seas overflow water around the basin. Consistent with the findings of Dickson and Brown (1994), this water is confined to densities greater than $\sigma_\theta = 27.8$ kg m^{-3} (and depths greater than 1500 m; Fig. 2b). Since the sill depth of Davis Strait to the north is much shallower than this (approximately 600 m), the

[2] It should be noted that the winter of 1997 was milder than those of the early 1990s, suggesting that convection along the boundary was more pronounced earlier in the decade.

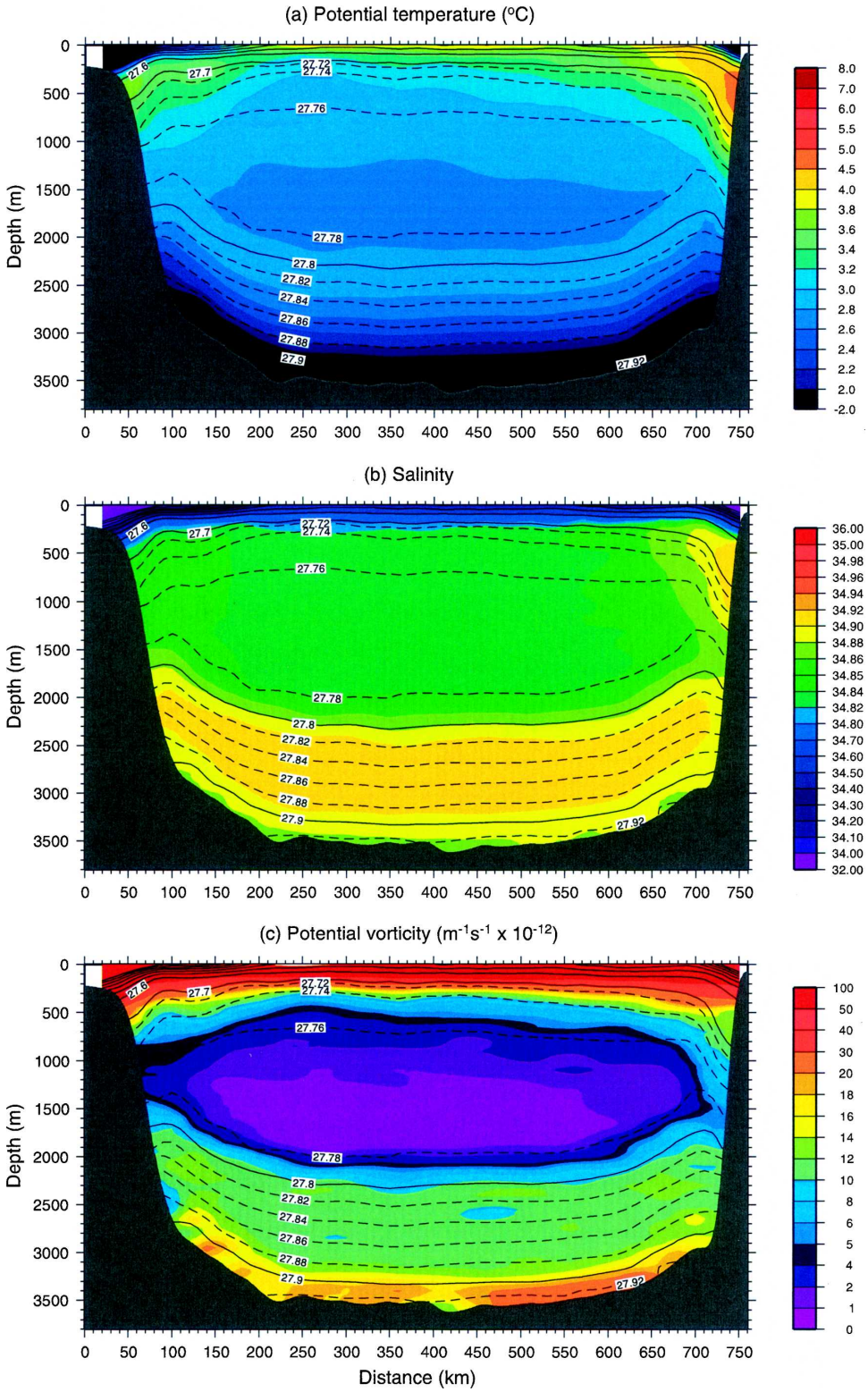

FIG. 2. Mean vertical sections (color) of (a) potential temperature, (b) salinity, and (c) planetary potential vorticity constructed from the 10 occupations of AR7W with potential density contours overlaid (kg m^{-3}). The Labrador shelf is on the left, and the Greenland shelf is on the right.

net transport across the AR7W line in this density layer should be zero. However, this is not the case for the absolute geostrophic velocity section calculated above, which has roughly 2 Sv more southward transport in this layer. This is perhaps not surprising because the continental slope is much steeper on the eastern side of the basin, which tends to channel and accelerate the flow (e.g., Eden and Böning 2002; Katsman et al. 2004), which in turn makes it more difficult to sample with floats. Accordingly, we forced the transport in the overflow layer to balance exactly by adjusting the eastern boundary current portion of the PALACE float lateral velocity profile at 700 m. In particular, an offset of 1.75 cm s^{-1} was applied for $x \geq 620$ km.

After this adjustment was made and applied to the geostrophic velocity section, not only did the transport in the overflow layer ($\sigma_\theta > 27.8$ kg m^{-3}) balance, but the net transport across the entire section balanced to within 0.1 Sv. This is rather remarkable, since the total inflow and outflow is 35.5 Sv. We believe that this is not a coincidence and that the (adjusted) mean velocity section accurately captures the balanced circulation in the Labrador Sea seaward of the shelf break. There is of course a net volume flux through the sea due to the outflow from Davis Strait, which means a complete section from the coast of Labrador to the coast of Greenland should be out of balance by this amount. However, this imbalance presumably occurs within the inshore, shallow regions not sampled by our mean velocity section (i.e., inshore of the 700-m isobath).

To demonstrate this we considered the data from a 3-yr mooring array across Davis Strait (Ross 1992). The mean meridional velocity (normal to the array line) was gridded in the same manner as the AR7W section. This included extrapolation over the top 150 m (above the shallowest current meters), which was done with the Laplacian-spline routine used earlier. Then, using a summertime hydrographic section occupied during the Davis Strait field program, we calculated the volume transport versus density class (realizing that the hydrographic section is synoptic, while the mooring data are averaged).

The net southward transport through the strait calculated as such, excluding the West Greenland shelf (where there were no moorings), is 3.0 Sv. The bulk of this (2.8 Sv) is contained in the density layer from the surface to $\sigma_\theta = 27.55$ kg m^{-3}. In the mean AR7W section the transport in this layer is balanced, that is, the inflowing transport equals the outflowing transport. We take this to mean that most of the Davis Strait throughflow is contained inshore of the 700-m isobath, consistent with the fact that the sill depth of the strait is approximately 600 m. Only 0.2 Sv of the outflow is denser than $\sigma_\theta = 27.55$ kg m^{-3}, which is on the order of the net imbalance in our section above the deep overflow layer (0.1 Sv). We note that Cuny et al.'s (2004) calculated net transport through Davis Strait is slightly different than the value computed here, since they used a more sophisticated extrapolation routine in the shallow layer and also extrapolated over the West Greenland shelf. However, this does not impact our conclusion because these regions are very shallow (i.e., it would just alter the component of transport less than $\sigma_\theta = 27.55$ kg m^{-3} inshore of the 700-m isobath). Also, the seasonality of the transport through the strait is fairly small in light of the uncertainties in the velocities (Cuny et al. 2004). Hence, our comparison between the mean Davis Strait conditions and the predominantly springtime AR7W composite is meaningful. We note that the calculations presented below of the overturning cell and horizontal gyre in the Labrador Sea, as well as the heat flux, rely on such a net balance of mass in the AR7W velocity section.

The mean velocity section (Fig. 3a) shows the inflowing West Greenland Current and outflowing Labrador Current near the shelf break in the upper layer (shallower than 1000 m), and the bottom-intensified Deep Western Boundary Current at the base of the continental slope (deeper than about 2000 m). Offshore of this the flow reverses, corresponding to the recirculations discussed in Lavender et al. (2000; see the schematic in Fig. 1). The deep flow reversal (to the south) adjacent to the eastern boundary near $x = 730$ km is curious and is the result of the strong lateral shear in the density field on this side of the basin (Fig. 2). This reversal amounts to 0.6 Sv, most of it contained in the overflow layer; hence it does not impact our subsequent calculations. Furthermore, it is associated with significant temporal variability (see below). Interestingly, a similar deep flow reversal was found in the Aguhlas Current system east of Africa (Beal and Bryden 1997).

Most of the observational studies to date of the Labrador Sea circulation have been conducted on the Canadian side of the basin, and the features seen on the western side of our mean velocity section are in line with these previous results. Most notably, Fischer et al. (2004) present mean vertical sections of alongslope velocity in the vicinity of the western boundary near 53°N (roughly 300 km south of the AR7W line). They constructed three different fields: a mean lowered acoustic Doppler current profiler section from six crossings between 1996 and 2001; a mean absolute geostrophic velocity section (referenced using moorings and floats) from the same six crossings; and a 2-yr mean section (1997–99) from a current meter array. All three sections were similar, showing the same general features noted above. The boundary circulation in these sections

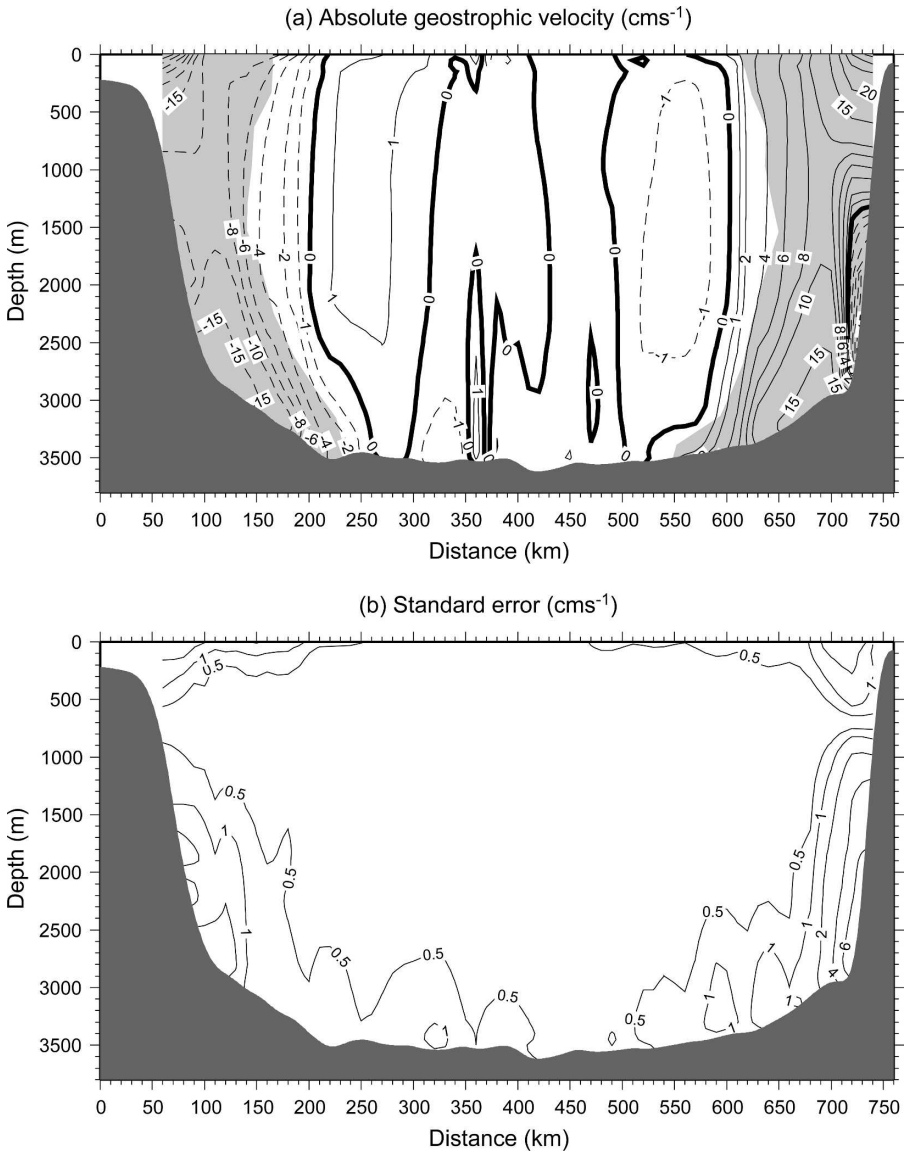

FIG. 3. (a) Mean absolute geostrophic velocity section adjusted to balance mass. Positive velocities (solid contours) are poleward, and negative velocities (dashed contours) are equatorward. The shaded regions are the throughput component of the boundary current (see text for details). (b) Section of the velocity standard error.

consists of the surface-intensified Labrador Current (30–35 cm s^{-1}) and bottom intensified Deep Western Boundary Current (15–20 cm s^{-1}), with weaker flow at middepth (10–15 cm s^{-1}). These speeds are a bit larger than in our mean section (Fig. 3a), but this is not surprising because the AR7W station spacing was larger, and point current-meter measurements tend to be larger than geostrophic estimates. The moored measurements of Lazier and Wright (1993), taken close to the AR7W line between 1978 and 1988, provide less coverage in the vertical but give a consistent view of the boundary current structure. The northward flow reversal on the western side of our section is seen as well in the Fischer et al. (2004) mean sections at a similar offshore location, and Lazier and Wright (1993) show a vanishingly small velocity at a comparable distance from the coast. However, Fischer et al. (2004) show a generally stronger recirculation than in Fig. 3a, and Lazier and Wright's (1993) farthest offshore mooring in the basin shows weak southward flow.

b. *Boundary current transport*

The equatorward transport on the western side of our mean AR7W section cannot be compared directly

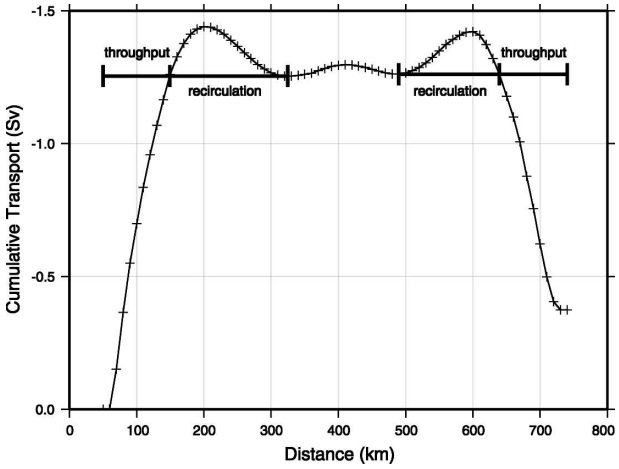

FIG. 4. Cumulative transport in the density layer σ_θ = 27.74–27.752 kg m^{-3} vs distance, which demonstrates the manner in which the boundary current throughput is distinguished from the recirculation.

with that of Fischer et al. (2004) because our section does not extend onto the shelf. However, for the part of the water column denser than σ_θ = 27.74 kg m^{-3} (corresponding to Fischer et al.'s deep-water layer) we get 22.9 Sv, comparable to Fischer et al.'s (2004) values of 25.4 Sv (lowered Doppler), 23.2 Sv (absolute geostrophic), and 25.2 Sv (moorings). An interesting and important feature of our mean velocity section is that the velocity in the central portion of the basin, between the recirculating gyres, is near zero (except the near-bottom flow near x = 300–400 km). This allows us to objectively separate the boundary current throughput from the recirculating transport. This was done as follows. For a series of density layers spanning the water column, we computed the cumulative transport originating from the western boundary. An example for one of the layers is shown in Fig. 4. The increase in southward transport as one progresses from the western side of the basin is due to the boundary current. We assume, however, that the seawardmost part of this transport increase—that which balances the subsequent transport decrease—is the onshore limb of the recirculation, that is, not part of the boundary current (see Fig. 4). The analogous criterion is applied at the eastern side of the basin. The boundary current throughput defined as such is denoted by the shaded regions in Fig. 3a. Note that this does not imply that the net transport in each of the individual density layers balances. As discussed later in the paper, above the deep overflow layer it does not (see, e.g., Fig. 4). However, it does suggest that any transport imbalances are predominantly confined to the boundary current regions.

The total boundary current throughput is 28.5 Sv. This is in line with other direct estimates that distinguish between the throughput and the recirculation [see the discussion in Pickart et al. (2002)]. Note, however, that our section does not capture the inshore, shallow parts of the West Greenland Current and Labrador Current, so the complete boundary current transport is greater than this. The deep component of the boundary current corresponding to the overflow water is 12.4 Sv, slightly less than the value of 13.3 Sv quoted by Dickson and Brown (1994) for the southern tip of Greenland (which is based on short-term moorings and a synoptic hydrographic section). The nearly barotropic recirculations on each side of the basin transport 2.5 Sv, respectively. Keep in mind that that the AR7W section does not cross the strongest part of this recirculating flow (Lavender et al. 2000; Fig. 1). Finally, in the overflow layer there is the deep recirculation near the eastern boundary and the small near-bottom recirculation near x = 300–400 km, together accounting for approximately ±2 Sv.

c. *Velocity error estimate*

Individual occupations of the AR7W section often contain significant mesoscale variability. For example, north of the line on the eastern side of the basin is a region of enhanced turbulent kinetic energy (Heywood et al. 1994; Prater 2002), where the deep-reaching eddies known as Irminger rings are believed to be formed (Lilly et al. 2003; Eden and Böning 2002; Katsman et al. 2004). These eddies propagate to the south and can be sampled during the occupation of the AR7W line (A. Clarke 2000, personal communication). Also, mooring records on the western side of the basin reveal energetic velocity fluctuations on time scales of 20–40 days (Fischer et al. 2004). Such high-frequency variability could strongly influence the AR7W snapshots. Consequently, volume and heat flux estimates using synoptic sections in the Labrador Sea—and in many other regions of the World Ocean—could contain large errors.

One of the strengths of the present analysis is that our velocity section is a composite of 10 occupations spanning 8 yr and referenced using float data averaged over 4 yr. Not surprisingly, this reduces much of the mesoscale noise seen in the individual AR7W sections. Assuming that each occupation is an independent measurement, we computed the vertical section of standard velocity error obtained from referencing each of the individual sections (Fig. 3b). Note that this error results entirely from the baroclinic component of the flow, since we have only the single mean lateral float profile at 700 m (and by necessity the error will be identically zero at this depth). Overall the standard velocity error is small through the interior of the section (less than

0.5 cm s^{-1}), increasing to 2 cm s^{-1} in the shallow portions of the West Greenland and Labrador currents. The largest uncertainties (up to 6 cm s^{-1}) occur in the overflow layer, particularly near the eastern boundary—that is, in the Deep Western Boundary Current (and in the deep flow reversal noted above). This is not surprising since strong flow above a sloping bottom often generates bottom-trapped topographic Rossby waves, which are a source of significant synoptic variability (true for the subtropical Deep Western Boundary Current; see Pickart and Smethie 1993; Pickart 1995). Keep in mind that this study focuses on the part of the water column above the overflow layer. As a measure of the relevant transport uncertainty, we computed the time series of net deviation transport from the surface to $\sigma_\theta = 27.8$ kg m^{-3}, the standard error of which is 0.4 Sv.

To demonstrate the importance of having a composite average we did the following exercise. First, each individually referenced geostrophic velocity section was adjusted to have no net transport in the overflow layer. The resulting transport imbalances in the remaining portion of the water column ranged from 1.7 to 10.7 Sv (compared to 0.1 Sv for the composite section). Next we constructed a series of composite sections by adding each individual occupation, one by one, to the average (doing the referencing and adjusting after each addition instead of on the individual occupations). The idea was to determine how many sections were necessary to obtain a robust average. When the sections were averaged in sequential order of occupation (1990 to 1997), the overflow transport converged after about seven sections (Fig. 5a). However, the imbalance in upper-layer transport did not become negligible until nine sections were used (Fig. 5b). Next, we did the iterative composite by ordering the individual sections from best (i.e., least amount of upper-layer imbalance) to worst (largest upper-layer imbalance). In this case the overflow transport was more constrained, and the imbalance in upper-layer transport (temporarily) disappeared after four occupations (Fig. 5). This means that, even when having the luxury of knowing which sections contained the least amount of mesoscale noise, it still took four occupations of AR7W to balance the transport across the section, and adding one more section brought it out of balance again.

As a final exercise we considered 2000 random permutations of the 10 sections in order to quantify the scatter associated with different ordering. Note that any ordering of the same subset of sections gives the same result. The distribution of the maximum number of independent combinations has a bell-shaped curve—the most combinations occur when using five sections (252 such combinations). Using our 2000 random orderings

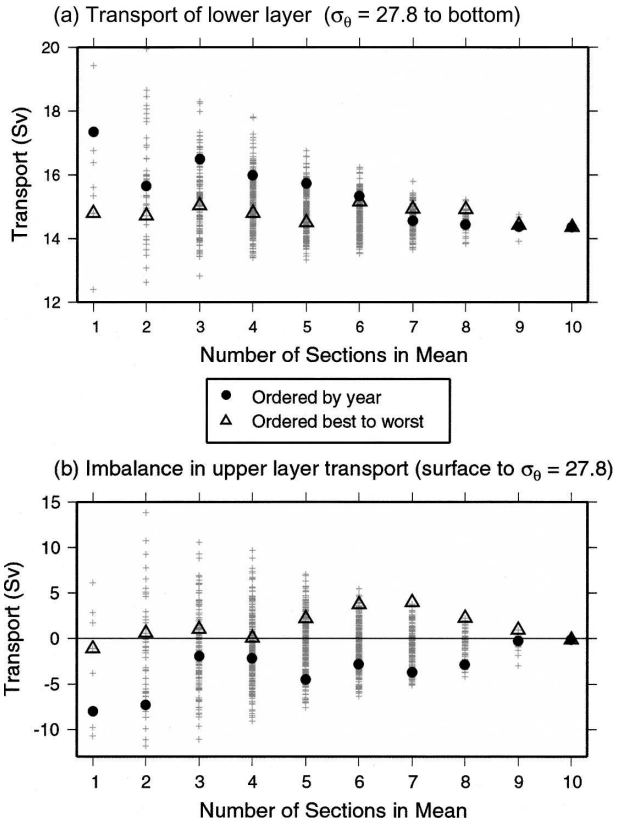

FIG. 5. (a) Transport into/out of the overflow layer as a function of the number of sections used in the composite average. The solid circles correspond to when the sections are added in sequentially by time, and the open triangles correspond to when they are added by order of decreasing individual transport imbalance in the upper layer. The gray plus symbols represent the scatter associated with different independent groupings of the sections (see text for details). (b) Transport imbalance in the layer above the overflow as a function of the number of sections used in the composite average. Symbols are the same as in (a).

of the sections, we realized 1022 of the 1023 possible independent groupings (missing only one grouping of five sections). Thus, we clearly obtained an accurate measure of the scatter. The point of this exercise was to get an idea of the minimum number of sections needed, out of a larger pool of ensemble members, to average out the mesoscale noise. Obviously one would have liked to have more sections, since by necessity the scatter goes to zero when the pool size is reached. However, it is encouraging that the scatter in transport—both the overflow layer volume flux and the upper-layer imbalance—became steadily smaller as more sections were used (Fig. 5). From the scatter one sees that the results are not especially robust when using small combinations of sections, but when more than seven occupations are used the variation becomes quite small. It is therefore clear that using our composite

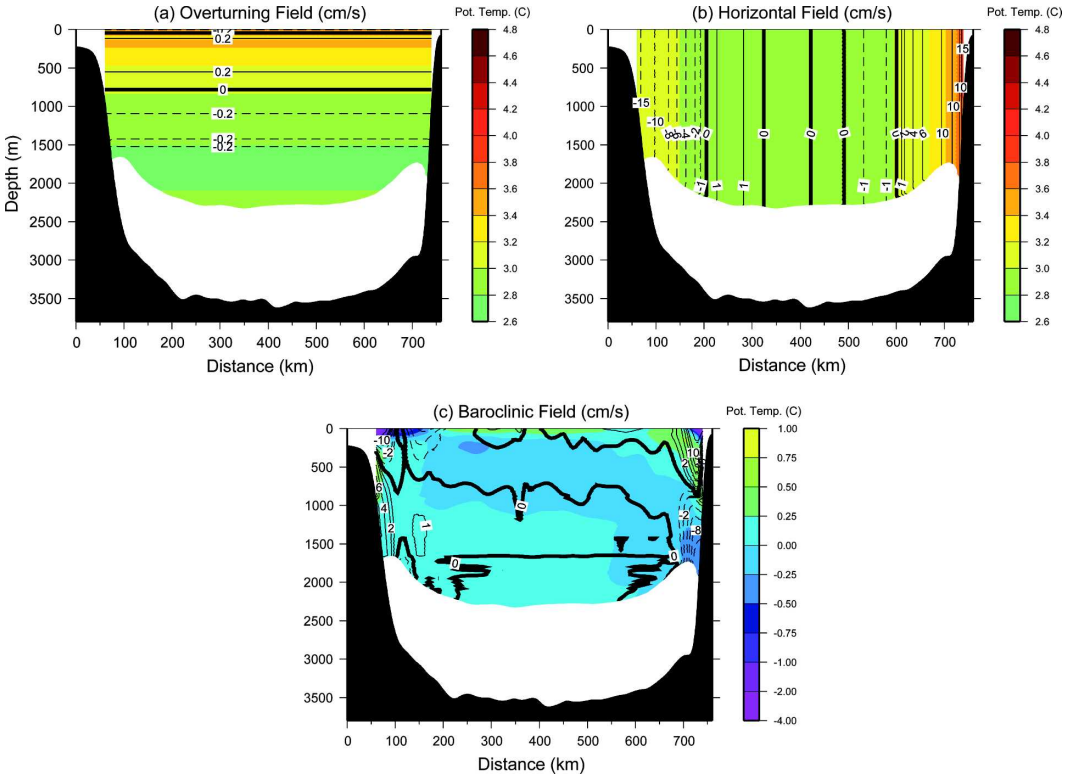

FIG. 6. Mean fields of velocity (contours) and potential temperature (color) corresponding to the decomposition in (1)–(2). The sign convention for velocity is the same as in Fig. 3. (a) Overturning field, (b) horizontal field, and (c) baroclinic field. The sum of these three components equals the full fields shown in Figs. 2a and 3a. The white shading is the overflow layer ($\sigma_\theta > 27.8$ kg m^{-3}), not considered in the analysis.

average significantly reduces the uncertainty inherent in typical synoptic sections from this part of the subpolar North Atlantic. It also highlights the importance of having repeat hydrography when addressing problems of this nature.

4. Overturning and horizontal components of the flow

a. Depth space

To separate the vertical and horizontal components of the Labrador Sea circulation, we followed the methodology of Fanning and Weaver (1997). In particular, the velocity (and other variables of interest such as temperature and salinity) was decomposed as follows:

$$v(x, z) = \overline{v(z)}^{x} + v'(x, z), \quad (1)$$

where $\overline{\ }^{x}$ represents an average along the section. The first term on the right-hand side of (1) is the overturning circulation, followed by the deviation velocity. The latter was then averaged vertically to obtain the horizontal gyre circulation along with the residual,

$$v'(x, z) = \overline{v'(x)}^{z} + \tilde{v}(x, z). \quad (2)$$

Following Fanning and Weaver (1997) the residual is referred to as the baroclinic gyre component. We note that the order of averaging in (1)–(2) could have been reversed (i.e., vertical averaging followed by lateral averaging), leading to the same result with this dataset.

The three components of velocity—the overturning cell, horizontal gyre, and baroclinic gyre—for the mean AR7W section are shown in Fig. 6, overlaid on the corresponding components of the temperature field. One sees immediately that to first order the circulation in the Labrador Sea is horizontal: the overturning cell is <1 cm s^{-1}, compared to the lateral gyre, which is >15 cm s^{-1}. The corresponding temperature fields indicate that warm water flows northward in the upper layer and cold water flows southward at depth (temperature difference $\Delta\theta \sim 0.5$°C), while warm water enters the basin on the eastern side and is cooled before exiting southward in the western boundary current ($\Delta\theta \sim 1$°C). The baroclinic gyre component consists of an upper-layer cyclonic boundary circulation situated above an anticyclonic circulation, with weak flow in the interior. In both layers the inflowing waters are warmer than the outflowing waters. (One should keep in mind that only

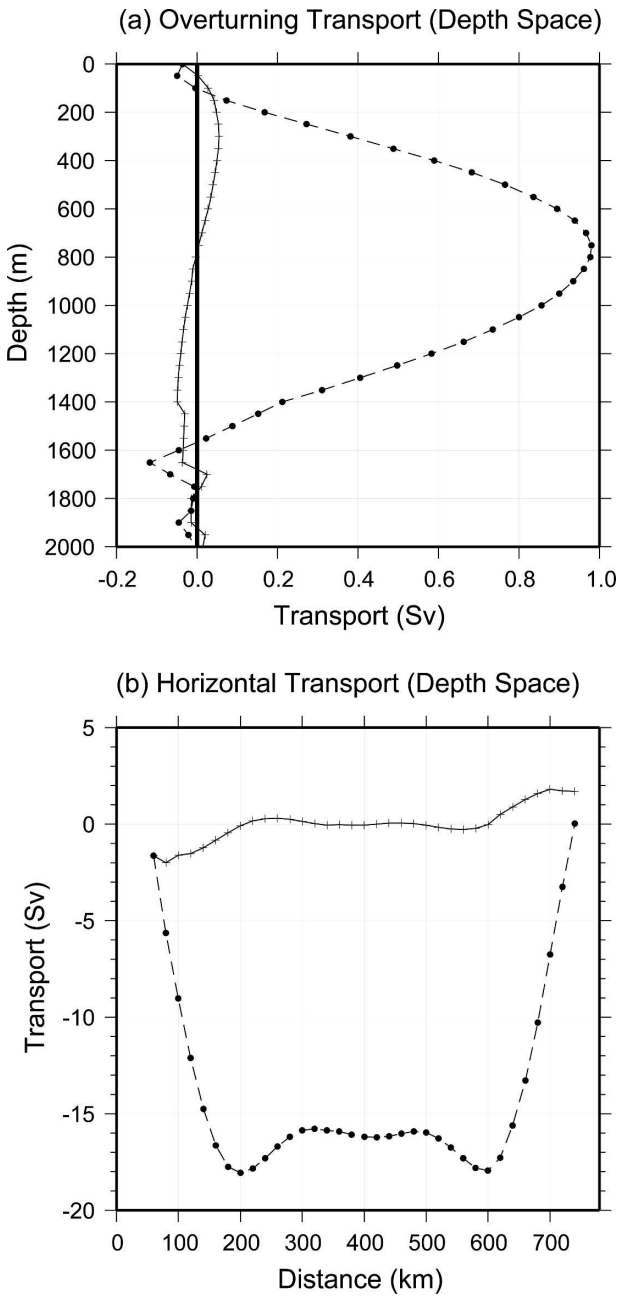

FIG. 7. (a) Overturning transport in depth space. The solid line with plus symbols denotes the values in the individual depth layers, and the dashed line with circles denotes the cumulative transport. Only every other point is plotted. (b) Same as in (a), but for the horizontal transport in depth space.

the temperature difference matters for the heat flux, not the absolute value of the temperature.)

The volume transports of the overturning and lateral cells are approximately 1 and 18 Sv, respectively (Fig. 7). The former is in agreement with the estimates of Spall and Pickart (2001; data applied to a theoretical estimate), Böning et al. (1996; high-resolution numerical model), and Straneo (2006; analytical model constrained by data). This indicates that very little net sinking is associated with convection in the Labrador Sea, and that its contribution to the North Atlantic MOC (13–15 Sv) is minor.[3] In Fig. 7a note that the cumulative transport curve is proportional to the vertical velocity profile of the overturning cell. The shape of this curve is consistent with the analytical quadratic profile of sinking obtained by Spall and Pickart (2001). Our observations indicate that the maximum downwelling associated with convection in the Labrador Sea occurs near 800 m. Furthermore, if we compute the sinking just within the region of the boundary current throughput (i.e., the analogous calculation confined to the shaded area of Fig. 3a), the estimate is within 5% of the value obtained for the entire section. This supports Böning et al's (1996) and Spall and Pickart's (2001) assertion that sinking in the subpolar gyre occurs predominantly near lateral boundaries.

b. *Density space*

As mentioned above, observational estimates of transformation in the Labrador Sea are more numerous than estimates of sinking, with values as large as 10 Sv. We calculated the diapycnal mass flux two ways: integrating within discrete density layers in the depth framework, and gridding the fields in density space. The two methods agree well, and since the latter offers better vertical resolution, we present the results in the density framework. Figure 8 shows the mean potential temperature and layer thickness fields gridded in density space. The scaled depth coordinate z' is obtained from the low-passed depth–density relationship using the interior portion of the mean σ_θ section. This allows us to plot the fields with a familiar depth/distance aspect ratio. The potential temperature (Fig. 8a) shows the same general features as in depth space (Fig. 2a). However, one can see that there are significant changes on density surfaces in the boundary current as it encircles the basin, most notably that nearly all the density layers become colder. The ramifications of this for heat flux are discussed in the next section. The layer thickness field (Fig. 8b) was computed by converting the regularly spaced scaled depth grid into density, differencing this in the vertical, and dividing by the mean

[3] Some of the LSW that is exported out of the basin is believed to get entrained into the overflow water south of Denmark Strait (e.g., McCartney 1992), and hence may contribute to the denser component of the MOC.

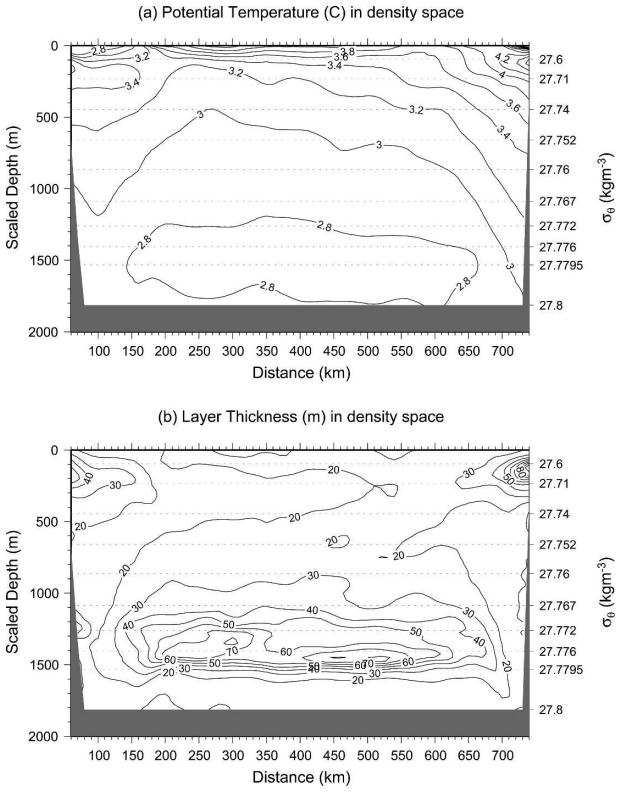

FIG. 8. Mean vertical sections constructed in density space. (a) Potential temperature and (b) layer thickness (see text for definition). The left-hand ordinate shows the scaled depth and the right-hand ordinate shows 10 representative density layers. The gray shading corresponds to the overflow layer (central portion of the section) or the bottom (near the boundaries).

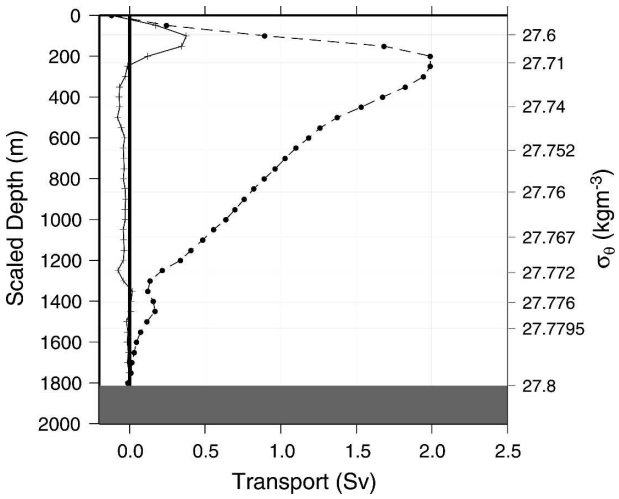

FIG. 9. Overturning transport in density space. The solid line with plus symbols denotes the values in the individual density layers, and the dashed line with circles denotes the cumulative transport. Only every other point is plotted. Other attributes of the plot are the same as in Fig. 8.

stratification. The largest layer thicknesses in the interior are associated with the newly convected LSW, consistent with the planetary potential vorticity distribution (Fig. 2c). Note that, as with temperature, there is also asymmetry in the layer thicknesses in the boundary current, with larger values on the eastern side of the basin.

Using the layer thickness field of Fig. 8b we computed the volume transport in density space. The overturning component of the transport, which measures the water mass transformation, is shown in Fig. 9. Note that the cumulative transformation is twice as large as the Eulerian sinking (2 Sv versus 1 Sv), indicating that half of the diapycnal mass flux in the Labrador Sea occurs in the horizontal plane. The value of 2 Sv is in line with several previous studies and is at the low end of the range quoted in the literature (Table 1). It also agrees well with the modeling results of Straneo (2006), who diagnosed 0.8 Sv of sinking versus 2 Sv of total transformation. [It should be noted that Straneo (2006) used our mean AR7W sections to specify various model parameters; hence Straneo's (2006) estimates are not independent from ours.] Note in Fig. 9 that the overturning cell in density space is asymmetric, with the center of the cell occurring at $\sigma_\theta = 27.71$ kg m^{-3}. This is approximately 700–900 m near the boundaries and 200 m in the interior (Fig. 2).

As was true in depth space, most of the transport imbalance leading to overturning in density space happens near the boundary (>95%). In the depth framework we interpreted this to mean that most of the net vertical sinking takes place near the boundary, because of the dynamical constraints discussed in Spall and Pickart (2001) and Spall (2004). In the density framework, however, there are no such constraints. At the same time, it is evident that water mass transformation does indeed occur in the interior (after all, this is where the deepest convection occurs in response to atmospheric heat loss). Hence it is not obvious how to interpret our result that the transport imbalance in density space occurs predominantly near the boundary; there are different possible scenarios.

For example, consider the extreme case in which the heat loss and transformation is confined mostly to the interior basin, such as in the models of Spall (2003) and Straneo (2006). In this case adiabatic exchange takes place via eddies, whereby cold, newly convected interior water continually enters the boundary current as it encircles the basin, and warm boundary current water enters the interior to balance the surface heat loss. A mean section across the basin (equivalent to AR7W) in this case could show all of the transport imbalance oc-

curring at the boundary, yet none of the transformation actually happened there. In the other extreme suppose that a large fraction of the transformation actually takes place in the boundary current, which is the case in the model of Spall (2004) where the atmospheric heat loss is distributed over the entire domain. Again, a section across this basin shows most of the imbalance occurring in the boundary current. In the Labrador Sea the strongest surface heat loss occurs in the western part of the basin seaward of the ice edge, that is, directly over the boundary current. Also, convection to 1200 m was observed in this part of the boundary current in the winter of 1996/97 (which was not a particularly harsh winter). We suspect, therefore, that much of the water mass transformation in the Labrador Sea does happen near the boundary. However, the precise breakdown—that is, what percentage of the 2 Sv calculated above gets transformed in the boundary current versus the interior—remains unknown.

5. Heat flux

Since the Labrador Sea is one of the few places in the North Atlantic where deep convection occurs, it is of considerable interest to know how much heat is fluxed northward as part of this process. Our dataset allows a meaningful calculation of this quantity since the mean velocity section balances mass. We again restrict our analysis to the part of the water column above the overflow layer. The total heat flux across this portion of the section is

$$\mathrm{HF} = \int_{h(x)}^{0} \int_{l_1(z)}^{l_2(z)} \rho(x,z) c_p(x,z) v(x,z) \theta(x,z)\, dx\, dz, \quad (3)$$

where v is the velocity, θ is the potential temperature, ρ is the in situ density, c_p is the specific heat of seawater, h is the height of the $\sigma_\theta = 27.78$ kg m^{-3} isopycnal (the top of the overflow layer), and l_1 and l_2 are the two lateral boundaries. Evaluating this integral gives a total northward heat flux across the Labrador Sea, seaward of the shelf break, of HF = 37.6 TW (1 TW $\equiv 10^{12}$ W).

We note that this is due to the mean geostrophic circulation only. That is, it does not include the contribution from the eddy flux of heat or the surface Ekman transport. We are unable to estimate the former (keep in mind that we have only a single mean PALACE float velocity composite for referencing), although the modeling results below suggest that this contribution is only $O(10\%)$. We can, however, estimate the heat flux contribution due to the surface Ekman transport. The wind stress was calculated using the seasonally averaged 10-m winds (May–June) for the period 1990–97 from the National Centers for Environmental Prediction (NCEP). During late spring/early summer weak low pressure exists over the central Labrador Sea and the associated winds are on the order of 2–3 m s^{-1}, generally oriented across the AR7W section. The corresponding Ekman flux is northward and very weak, less than 0.01 Sv (although admittedly the NCEP spatial resolution of 2.5° is poor for this calculation). This implies that the heat flux due to the Ekman transport is negligible for the AR7W section.

Does the northward heat flux in the Labrador Sea balance the loss of heat to the atmosphere north of the section? To answer this we assume that the annual average heat flux across the AR7W line is approximately 70% of the value obtained from our predominantly springtime composite. This is suggested by the modeling results in the next section and gives an annual mean heat flux of 26.3 TW. Next we computed the annual average ocean-to-atmosphere total heat flux north of the line for the years 1990–97 using the adjusted NCEP product of Renfrew et al. (2002), where the total heat flux is the sum of the sensible, latent, and shortwave and longwave radiative terms. (We assume that there is negligible heat loss in Davis Strait and Baffin Bay due to the ice cover that is present over much of the year.) This average is 15.2 TW, which implies that we cannot account for nearly half of the annual heat flux across AR7W. However, the coarse resolution of NCEP together with the complexity of the ocean-atmosphere system in this region, including the presence of sea ice in winter over the western Labrador shelf, suggests that our heat loss calculation is suspect.

Consider that the annual mean heat loss measured at the Bravo mooring site (Fig. 1) for 1972 was 154 W m^{-2} (Pickart et al. 1997). While the winter of 1972 was particularly harsh, keep in mind that the early 1990s were characterized by the highest NAO index, and the deepest convection, in the historical record. If we assume that the annual heat loss at the Bravo site during this period was two-thirds the value in 1972 and apply it over a 500-km^2 region north of the AR7W line (which encompasses the area of deep convection), we are able to balance the annual AR7W heat flux of 26.3 TW. Clearly the precise budget still needs to be quantified, but this demonstrates that our calculated AR7W heat flux is not unreasonable in light of what should be required to balance the heat loss to the atmosphere via deep convection.

a. Components in depth space

We also computed the heat flux associated with the different components of the circulation: the overturning cell, lateral gyre, and baroclinic gyre (Fig. 6). Here

it is assumed that the in situ density and specific heat are constant, and the decomposed potential temperature and velocity are used in an integral akin to (3). As a check on our calculations, each integral was also computed using a constant temperature field to make sure that the resultant heat flux was near zero. Not surprisingly, based on the discrepancy in magnitude between the overturning and lateral cells (Fig. 7), the dominant contribution to the heat flux in the Labrador Sea is due to the lateral circulation, 25.5 TW (70.2%). The overturning cell fluxes only 1.7 TW (4.7%), while the remainder is due to the baroclinic gyre, 9.1 TW (25.2%). The sum of these terms is 36.4 TW, which is slightly less than the value obtained using the full fields (37.6 TW), reflecting numerical error in our decomposition. It is worthwhile to mention that these results are insensitive to the choice of reference level for the potential temperature. To demonstrate this, we did the same set of calculations using a deep reference level of 2500 dbar (as opposed to the sea surface). In this case temperatures were warmer throughout the water column by 0.15°–0.25°C. The total heat flux through the section differed by only 2%, and the percentage breakdown between the overturning, horizontal, and baroclinic gyre components was identical. This insensitivity is due to the fact that the mean AR7W section balances mass.

b. Components in density space

Using a global dataset, Talley (2003) calculated that the Labrador Sea overturning cell transports 7 Sv in density space, and that this is associated with a heat transport of 350 TW. These values seem at odds with our results, but there are several points to consider. The northernmost section in the North Atlantic used by Talley (2003) was occupied in March–April 1962 and was situated near 59.5°N. In the Labrador Sea this is northward of where most of the convection takes place (Clarke and Gascard 1983; Pickart et al. 2002). Furthermore, 1962 was during a period when the NAO index was near zero to negative, which is not conducive for convection in the Labrador Sea (Dickson et al. 1996). Hence it is not entirely appropriate to compare our results with Talley's (2003), since most of the transformation discussed in that paper seems to happen outside of the Labrador Sea. It should also be kept in mind that there is a large uncertainty in Talley's (2003) estimate, due in part to synopticity of the measurements and partly because the velocities were not directly referenced.

Nonetheless, the impression one gets from Talley's (2003) study is that most of the heat flux calculated in the density framework in the subpolar North Atlantic is associated with the overturning cell. We find that this is not the case in the Labrador Sea, at least during the period of strong convection in the early 1990s. The northward heat flux corresponding to the 2-Sv overturning cell in Fig. 9 is 3.9 TW, which implies that only 10% of the total heat flux is due to the diapycnal mass flux resulting from convection in the Labrador Sea. This in turn indicates that a large fraction of the heat flux in density space is accomplished by transformation within density surfaces; that is, the water gets colder and fresher as it encircles the basin, with a large degree of density compensation. This happens because near-surface freshwater, which originates from the boundary and spreads into the interior during the course of the year, gets mixed into the water column during the wintertime overturning. The degree of θ/S compensation can be seen by considering the distribution of properties along a density layer in the upper part of the water column (Fig. 10). As one progresses from the eastern boundary to the western boundary, the layer gets fresher by 0.1 and colder by 1°C. Note also that the layer thickness decreases by roughly 300 m from the eastern boundary current to the western boundary current.

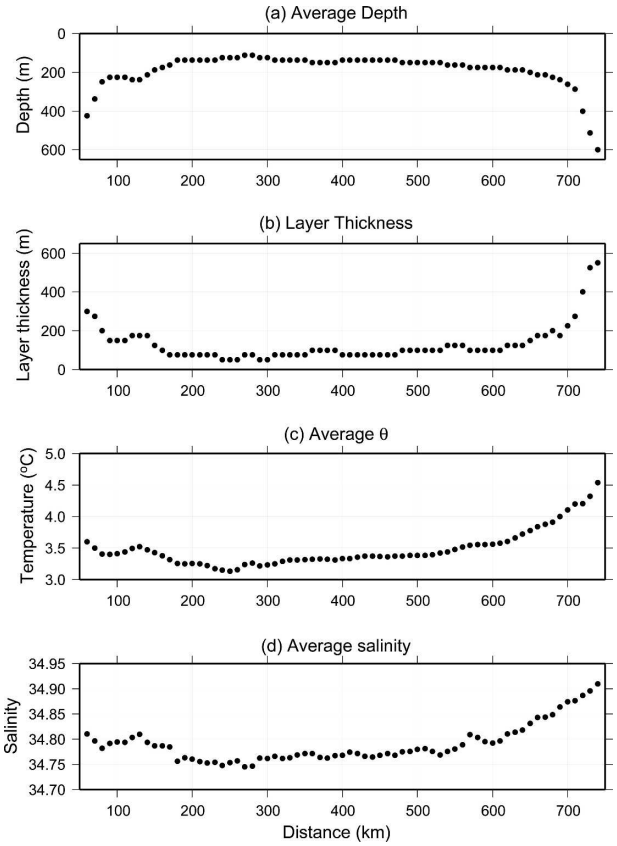

FIG. 10. Properties averaged within the density layer $\sigma_\theta = 27.6$–27.72 kg m^{-3}: (a) average depth, (b) layer thickness, (c) average potential temperature, and (d) average salinity.

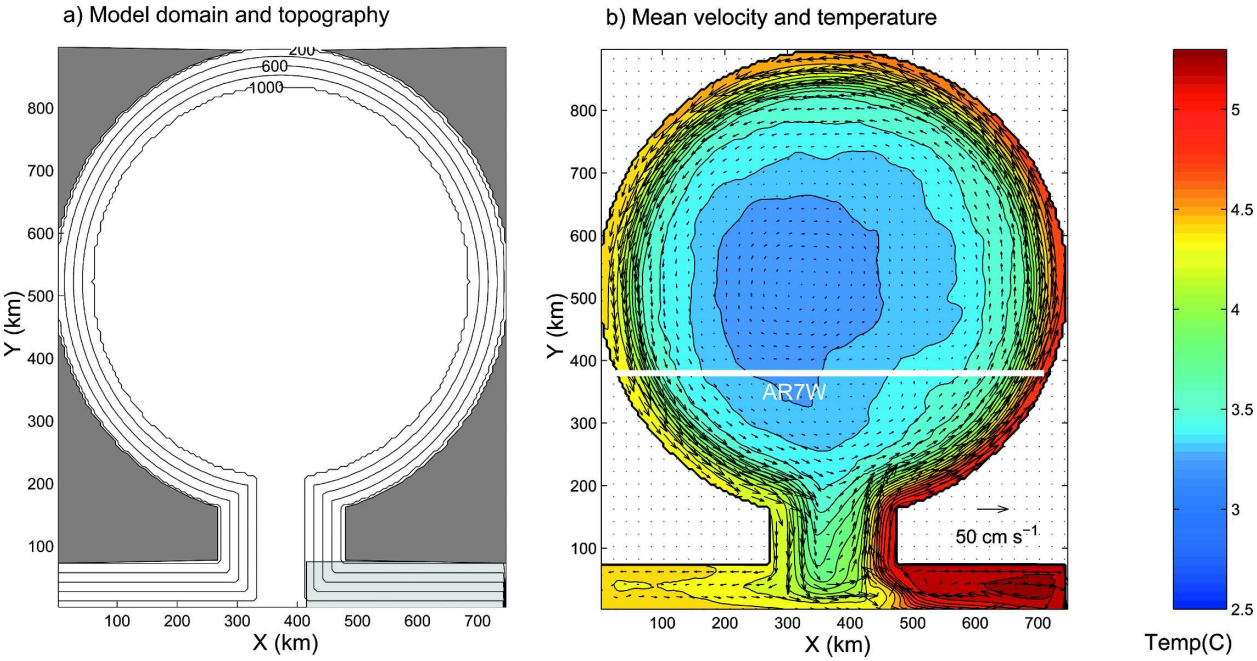

FIG. 11. (a) Model domain and bottom topography (m). The model temperature is restored toward 5°C throughout the water column within the lightly shaded region. (b) Model velocity vectors (every fourth grid point) and temperature (color) averaged over the final 5 yr of integration at 50-m depth. The location of a section analogous to the AR7W line is indicated by the white line.

It seems then that the proximity of the Labrador Sea to major sources of freshwater (Hudson Bay and the Arctic), the seasonality of the freshwater cycle, and the ability of the freshwater to spread into the interior significantly impact the mechanisms by which heat is fluxed northward into the sea. If salinity did not play such an active role, that is, if the temperature distribution predominantly dictated the density, then most of the heat flux would of course be accomplished by the density overturning cell. As a way to demonstrate this we calculated the overturning transport and heat flux in temperature space. As in the depth and density framework, mass is conserved when integrated over the overturning cell, whose strength in temperature space is 7.5 Sv. The associated heat flux is 35.0 TW, as compared with the integrated value from (3) of 37.6 TW. These are not distinguishable within the error bar (computed as above), which is somewhat larger for this calculation because of the large temperature gradients in the upper layer. This result highlights further the degree to which θ/S compensation impacts the nature of the heat flux in the Labrador Sea.

6. Overturning and heat flux in an idealized model ocean

The use of repeat hydrographic sections for the data analysis reduced the errors associated with mesoscale variability in the synoptic data, but there was not sufficient temporal coverage to resolve either the seasonal cycle or the eddy heat flux across the section. We now use results from an idealized eddy-resolving model of a marginal sea to augment the previous analysis. While the model is not intended to represent the actual Labrador Sea, it does provide a complete and consistent reference solution and a means to access the average heat transport, the magnitude of the eddy heat flux, and the seasonal cycle in heat transport in a basin that produces a similar boundary current structure and convective water mass.

The model run presented here was previously described in Spall (2004) and will be only briefly outlined now. The domain consists of a nearly closed basin with a sloping bottom over the outer 60 km (representing a marginal sea) that is connected to an "open ocean" by a 200-km-wide strait (Fig. 11a). The temperature is restored toward a uniform stratification within the open ocean in order to provide a source of warm water. Heat loss of 120 W m^{-2} is applied to the marginal sea for a period of two months and turned off for 10 months. This annual cycle is repeated for a period of 25 yr. The analysis here is taken from the final 5 yr of integration. The model has 5-km horizontal resolution and 10 levels in the vertical uniformly distributed over 1000-m depth. Details of the model calculation and a discussion of the

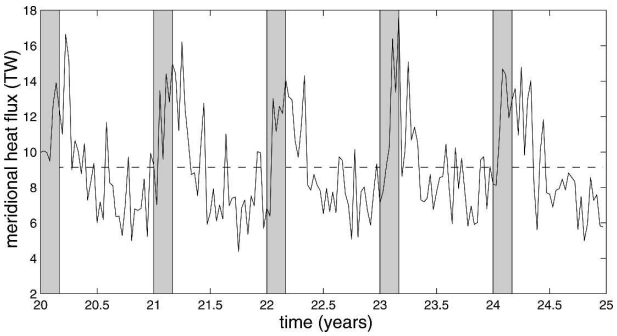

FIG. 12. Advective heat flux into the model domain across a section at $y = 150$ km for the final 5 yr of model integration. Uniform cooling of 120 W m^{-2} is applied over the model domain for two months each year, indicated by the shaded bars. The mean heat flux is given by the dashed line.

physics that controls the circulation and water mass properties can be found in Spall (2004).

The mean temperature and horizontal velocity at 50-m depth over the final five years of integration are shown in Fig. 11b. The circulation is dominated by a strong, narrow cyclonic boundary current with velocities $O(25\ \text{cm s}^{-1})$. The warm inflowing waters are cooled as they encircle the basin. The interior of the domain is filled with dense, weakly stratified water and a weak, anticyclonic circulation. As discussed in Spall (2004), the heat loss in the interior is balanced by eddy fluxes from the boundary current. The strength of the boundary current is determined by the amount of baroclinic shear required to provide the eddy fluxes that can balance the surface cooling in the interior. The advective heat flux into the marginal sea (at $y = 150$ km) over the final five years of integration is shown in Fig. 12. The cooling period is indicated by the shaded regions at the beginning of each year. The largest heat flux occurs near the end of the cooling period and persists for approximately 2 months after the cooling has ceased. The heat flux during the remainder of the year is still significant, although only about one-half of its peak value. This suggests that the late-spring occupation of AR7W is well-timed for measuring the heat flux into the Labrador Sea.

The total advective heat flux into the marginal sea is 9.1 TW, with 8.7 TW due to the mean velocity advecting the mean temperature, and 0.4 TW due to the time-dependent correlation between velocity and temperature. This time-dependent flux is not due to coherent eddies but is instead a result of the peak velocities in the boundary current coinciding with a larger temperature difference between the inflow and outflowing boundary current water. At the midlatitude of the basin the eddy heat flux integrated across the basin is essentially zero. This is not surprising given the symmetry in the domain and forcing; any section passing through the middle of the basin would be expected to have a very small eddy heat flux since the eddies are fluxing heat toward the center of the basin. For a section that is offset to the south, equivalent to the AR7W line (Fig. 11b), the heat flux is also dominated by the mean heat advection (88% of the total). This suggests that the eddy heat flux across AR7W is small, as was assumed in the data analysis above. Note that this does not mean that the eddy heat fluxes are small everywhere in the basin. In fact, the eddies are entirely responsible for balancing the surface cooling within the interior of the marginal sea. It is just that they are directed from the boundary into the interior so that they will tend to be parallel to any section that crosses the basin.

As was done for the observations, the model velocity and temperature fields have been decomposed into the overturning, horizontal, and baroclinic gyre components. The resulting fields shown in Fig. 13 compare well to those calculated from the data (Fig. 6), both in terms of magnitude and pattern. The velocity is dominated by the horizontal gyre of $O(15\ \text{cm s}^{-1})$ and the temperature anomalies are concentrated near the boundaries. The overturning gyre is very weak, less than 0.5 cm s^{-1}. The decomposition for heat flux, based on these components, shows similarly good agreement with the observations.

The strength of the horizontal and overturning cells can be understood by a theoretical consideration of the heat and mass budgets of the basin and the dynamics that control the heat exchange between the boundary current and the interior (see Spall 2004). For the circular basin considered here, a key parameter is $\varepsilon = 2\pi Rc/L$, where R is the radius of the basin, L is the width of the topography, and $c = 0.025e^{2\delta}$ is an efficiency coefficient that regulates the eddy heat flux from the boundary current into the interior. The parameter δ is the ratio of the topographic slope to the isopycnal slope. For a cyclonic boundary current $\delta < 0$, and the topography acts to stabilize the boundary current and reduce the amount of eddy flux into the interior. For the model calculation above, $\varepsilon \approx 0.15$. It is difficult to determine ε accurately for the Labrador Sea, but for typical isopycnal and topographic slopes in Fig. 2, $\delta \approx -0.25$ and $\varepsilon \approx 0.2$. The parameter ε is the ratio of the heat flux carried into the interior by eddies to the heat flux carried by the boundary current. The theory of Spall (2004) showed that, for $\varepsilon \ll 1$, the amount of downwelling in the marginal sea is given by $0.5\varepsilon M$, where M is the baroclinic transport in the boundary current. For the Labrador Sea $M = 8.3$ Sv, which was

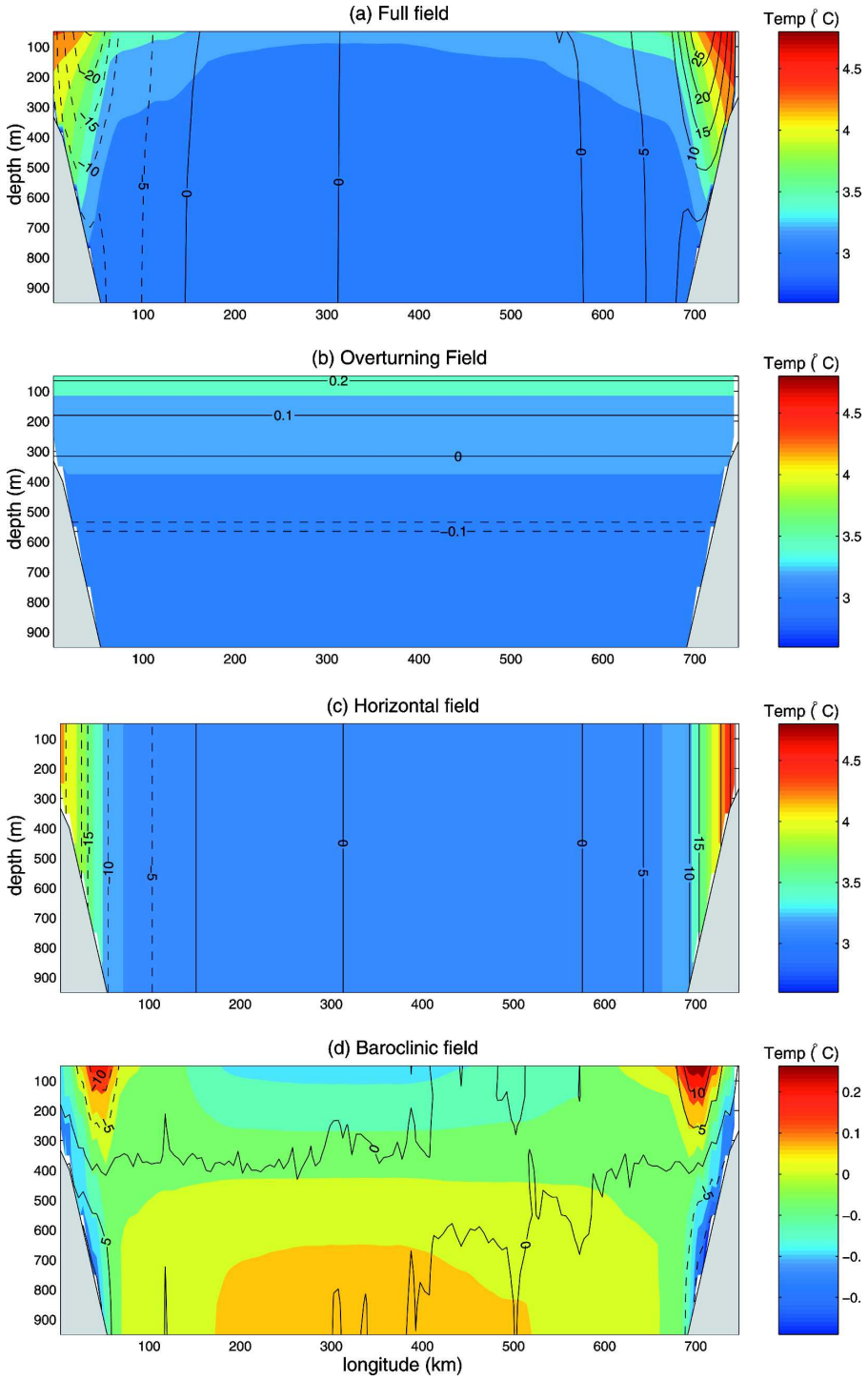

FIG. 13. Components of the mean model velocity (contours; cm s^{-1}) and temperature (color; °C) at the midlatitude of the basin (y = 525 km). The sign convention for velocity is the same as in Fig. 3. Shown are the (a) full velocity and temperature field, (b) overturning field, (c) horizontal field, and (d) baroclinic field (where the mean temperature of this component has been subtracted out).

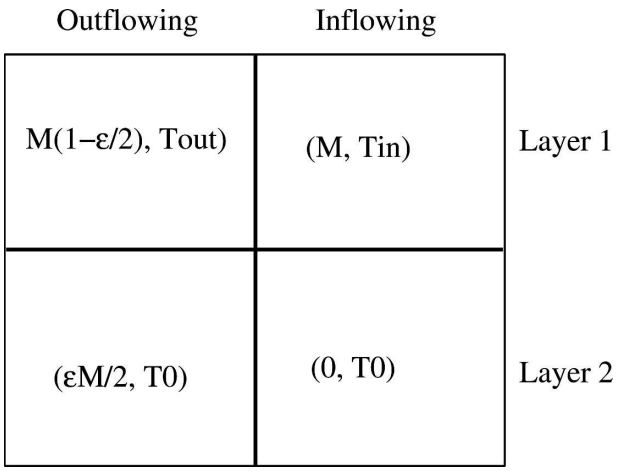

FIG. 14. Schematic of the two-layer, four-box model representation of the boundary current system. The inflowing transport is M, and the temperature of the inflowing water is T_{in}. The outflowing transport in the upper layer is reduced, and the deep layer transport is increased, by $\varepsilon/2M$. The outflowing water in the upper layer is slightly cooler than the inflowing water, with temperature T_{out}.

calculated from the observations using the top of the overflow layer ($\sigma_\theta = 27.8$ kgm^{-3}) as a reference level of no motion. For this value of M the theory predicts a downwelling within the Labrador Sea of 0.83 Sv, in close agreement with the value of 1 Sv deduced from the data.

The theory can also be used to estimate the breakdown of the heat transport into the horizontal, overturning, and baroclinic components. Motivated by analysis of the eddy-resolving model and the above data analysis, it is illustrative to assume that the heat transport into the basin is controlled by the boundary currents and that the inflowing and outflowing currents can be represented by two layers. This system can be described by four boxes, as indicated in Fig. 14. The inflowing transport is M and has a temperature relative to the temperature of the LSW of $T_{in} - T_0$. The theory in Spall (2004) can be used to relate the outflowing temperature and transport to the inflowing temperature, transport, and ε. The outflowing transport in the upper layer is $M(1 - \varepsilon/2)$ and has a temperature anomaly of $T_{out} - T_0 = (T_{in} - T_0)(1 - \varepsilon)$. The outflowing waters are slightly cooler than the inflowing water and the transport in the upper layer is slightly less. Because of the downwelling within the basin, the deep layer has a transport of $M\varepsilon/2$ and has a temperature equal to that of the LSW, T_0. For simplicity, it has been assumed that the inflowing transport in layer 2 is zero. A nonzero deep inflowing transport would increase the heat transport by the horizontal gyre; thus the present estimate provides a lower bound for the horizontal gyre heat transport and an upper bound for the overturning heat transport.

The heat transport carried by each component can be calculated from the transports and temperature anomalies in Fig. 14. The total heat transport into the basin is $HF_{theory} = M(T_{in} - T_{out}) + 0.5\varepsilon M(T_{out} - T_0) = \varepsilon M(3/2 - \varepsilon/2)(T_{in} - T_0)$. The final relation can be derived using the results of Spall (2004). To within $O(\varepsilon^2)$, the horizontal gyre equals $0.5H\,F_{theory}$, the baroclinic gyre equals $(0.5 - \varepsilon/2)HF_{theory}$, and the overturning cell equals $\varepsilon/2HF_{theory}$. For our estimate for the Labrador Sea ($\varepsilon = 0.2$), the breakdown is 50% horizontal, 40% baroclinic, and 10% overturning. Given the approximations required to derive this theoretical estimate, the comparison with the actual heat flux components (70.2% horizontal, 25.2% baroclinic, and 4.7% overturning) is reasonable. Consideration of the barotropic transport in the boundary current would result in an even larger heat transport for the horizontal gyre, in better agreement with the observations.

The horizontal gyre dominates the heat transport because the topography stabilizes the boundary current to such a degree that a strong boundary current is required in order to form enough eddies through baroclinic instability to transport heat into the basin interior to offset the atmospheric cooling. This strength is represented by the difference between the temperature (density) of the inflowing waters and that of the interior LSW. It is this large boundary current transport, compared to the weak downwelling (due to the baroclinic instability and a viscous boundary layer; Spall 2004) that is responsible for the dominance of the horizontal gyre in heat transport. As the exchange parameter ε increases, the contribution from the overturning increases while the baroclinic gyre contribution decreases (the horizontal gyre component remains near 50% of the total). However, in the extreme limit of $\varepsilon > 1$, the boundary current disappears before it encircles the basin because of the large eddy fluxes into the interior. In this case the horizontal gyre component vanishes and the overturning cell dominates the heat flux. This clearly is not the case in the Labrador Sea, although it may apply to large basins such as the Mediterranean Sea.

7. Conclusions

Using a composite vertical section of absolute geostrophic velocity across the Labrador Sea—referenced using float data and adjusted to balance mass—we have inferred the overturning circulation in depth space (net sinking) and density space (net water mass transformation). Our study focused on the time period 1990–97,

corresponding to a period of especially high NAO index. Despite the fact that the wintertime convection in the Labrador Sea during this period was the deepest and densest ever recorded, the calculated sinking was only 1 Sv, and the diapycnal transformation only 2 Sv. Furthermore, most of the transport imbalance, in both cases, occurred near the lateral boundaries of the basin. The horizontal circulation was found to be much greater, 18 Sv, and was responsible for most of the northward heat flux (approximately 70% of the calculated 37.6 TW). Even in density space only a small fraction of the heat flux (approximately 10%) was due to the overturning. This is because of the large degree of θ/S compensation associated with the Arctic-origin freshwater signal in the Labrador Sea.

These results suggest that the North Atlantic MOC is not significantly impacted by wintertime convection in the Labrador Sea. However, one must keep in mind that some amount of convection does occur south of the AR7W line (see Pickart et al. 1997), although it appears that the deepest mixed layers are north of the section (Clarke and Gascard 1983; Pickart et al. 2002). Another possible contribution to the middepth component of the MOC, not captured in this study, could be due to convection in the Irminger Sea on the eastern side of Greenland. Recent studies have indicated that deep overturning occurs there (Bacon et al. 2003; Pickart et al. 2003b; Centurioni and Gould 2004; Våge et al. 2007), likely due to the atmospheric forcing of the Greenland tip jet (Doyle and Shapiro 1999; Pickart et al. 2003a,b; Moore and Renfrew 2005). A composite vertical section across the southern Irminger Sea has been constructed for the same time period considered here (see Pickart et al. 2003a), which shows similarly strong east–west contrasts in temperature and salinity. We suspect that comparable sinking and transformation could occur in the Irminger Sea, perhaps making the total contribution to the MOC from both seas more significant. Future work will be aimed at quantifying this.

Acknowledgments. The authors thank the many scientists and technicians at the Bedford Institute of Oceanography who have worked tirelessly to keep the AR7W program going. They have provided, and continue to provide, the oceanographic community with an incredibly valuable dataset. This study is dedicated to two of these scientists: John R. N. Lazier and R. Allyn Clarke. Author RP is grateful to these outstanding researchers for many enlightening discussions and insightful input over the years on the oceanography of the Labrador Sea. They are two of the pioneers in the study of this fascinating and complex area of the ocean. This work was funded by the National Science Foundation through Grants OCE-0450658 (RP) and OCE-024978 (MS).

REFERENCES

Bacon, S., W. J. Gould, and Y. Jia, 2003: Open-ocean convection in the Irminger Sea. *Geophys. Res. Lett.,* **30,** 1246, doi:10.1029/2002GL016271.

Beal, L. M., and H. L. Bryden, 1997: Observations of an Aguhlas Undercurrent. *Deep-Sea Res. I,* **44,** 1715–1724.

Böning, C. W., F. O. Bryan, W. R. Holland, and R. Doscher, 1996: Deep-water formation and meridional overturning in a high-resolution model of the North Atlantic. *J. Phys. Oceanogr.,* **26,** 1142–1164.

Brandt, P., A. Funk, L. Czeschel, C. Eden, and C. Böning, 2007: Ventilation and transformation of Labrador Sea Water and its rapid export in the deep Labrador Current. *J. Phys. Oceanogr.,* **37,** 946–961.

Centurioni, L. R., and W. J. Gould, 2004: Winter conditions in the Irminger Sea observed with profiling floats. *J. Mar. Res.,* **62,** 313–336.

Clark, P. U., N. G. Pisias, T. F. Stocker, and A. J. Weaver, 2002: The role of thermohaline circulation in abrupt climate change. *Nature,* **415,** 863–869.

Clarke, R. A., and J. C. Gascard, 1983: The formation of Labrador Sea water. Part I: Large-scale processes. *J. Phys. Oceanogr.,* **13,** 1764–1778.

Cuny, J., P. B. Rhines, P. P. Niiler, and S. Bacon, 2002: Labrador Sea boundary currents and the fate of the Irminger Sea Water. *J. Phys. Oceanogr.,* **32,** 627–647.

——, ——, and R. Kwok, 2004: Davis Strait volume, freshwater and heat fluxes. *Deep-Sea Res. I,* **52,** 519–542.

Delworth, T., S. Manabe, and R. J. Stouffer, 1993: Interdecadal variations of the thermohaline circulation in a coupled ocean–atmosphere model. *J. Climate,* **6,** 1993–2011.

Dickson, R. R., and J. Brown, 1994: The production of North Atlantic deep water: Sources, rates, and pathways. *J. Geophys. Res.,* **99,** 12 319–12 341.

——, J. R. N. Lazier, J. Meincke, P. B. Rhines, and J. Swift, 1996: Long-term coordinated changes in the convective activity of the North Atlantic. *Prog. Oceanogr.,* **38,** 241–295.

Doyle, J. D., and M. A. Shapiro, 1999: Flow response to large-scale topography: The Greenland tip jet. *Tellus,* **51,** 728–748.

Eden, C., and C. Böning, 2002: Sources of eddy kinetic energy in the Labrador Sea. *J. Phys. Oceanogr.,* **32,** 3346–3363.

Fanning, A. F., and A. J. Weaver, 1997: A horizontal resolution and parameter sensitivity study of heat transport in an idealized coupled climate model. *J. Climate,* **10,** 2469–2478.

Fischer, J., F. A. Schott, and M. Dengler, 2004: Boundary circulation at the exit of the Labrador Sea. *J. Phys. Oceanogr.,* **34,** 1548–1570.

Hall, M. M., and H. L. Bryden, 1982: Direct estimates and mechanisms of ocean heat transport. *Deep-Sea Res.,* **29,** 339–359.

Heywood, K. J., E. L. McDonagh, and M. A. White, 1994: Eddy kinetic energy of the North Atlantic subpolar gyre from satellite altimetry. *J. Geophys. Res.,* **99,** 22 525–22 539.

Katsman, C. A., M. A. Spall, and R. S. Pickart, 2004: Boundary current eddies and their role in the restratification of the Labrador Sea. *J. Phys. Oceanogr.,* **34,** 1967–1983.

Lavender, K. L., R. E. Davis, and W. B. Owens, 2000: Mid-depth

recirculation observed in the interior Labrador and Irminger Seas by direct velocity measurements. *Nature,* **407,** 66–69.

Lazier, J. R. N., and D. G. Wright, 1993: Annual velocity variations in the Labrador Current. *J. Phys. Oceanogr.,* **23,** 659–678.

——, A. Clarke, I. Yashayaev, and P. Rhines, 2002: Convection and restratification in the Labrador Sea, 1990–2000. *Deep-Sea Res.,* **49,** 1819–1835.

Lilly, J. M., P. B. Rhines, M. Visbeck, R. Davis, J. R. N. Lazier, F. Schott, and D. Farmer, 1999: Observing deep convection in the Labrador Sea during winter 1994/95. *J. Phys. Oceanogr.,* **29,** 2065–2098.

——, ——, F. Schott, K. Lavender, J. R. N. Lazier, U. Send, and E. D'Asaro, 2003: Observations of the Labrador Sea eddy field. *Prog. Oceanogr.,* **59,** 75–176.

Marsh, R., 2000: Recent variability of the North Atlantic thermohaline circulation inferred from surface heat and freshwater fluxes. *J. Climate,* **13,** 3239–3260.

——, B. A. de Cuevas, A. C. Coward, H. L. Bryden, and M. Alvarez, 2005: Thermohaline circulation at three key sections in the North Atlantic over 1985–2002. *Geophys. Res. Lett.,* **32,** L10604, doi:10.1029/2004GL022281.

Mauritzen, C., 1996: Production of dense overflow waters feeding the North Atlantic across the Greenland-Scotland ridge. Part 1: Evidence for a revised circulation scheme. *Deep-Sea Res.,* **43,** 769–806.

——, and S. Häkkinen, 1999: On the relationship between dense water formation and the "Meridional Overturning Cell" in the North Atlantic Ocean. *Deep-Sea Res. I,* **46,** 877–894.

McCartney, M. S., 1992: Recirculating components to the deep boundary current of the northern North Atlantic. *Prog. Oceanogr.,* **29,** 283–383.

——, and L. D. Talley, 1984: Warm-to-cold conversion in the northern North Atlantic Ocean. *J. Phys. Oceanogr.,* **14,** 922–935.

McManus, J. F., R. Francois, J.-M. Gherardi, L. D. Keigwin, and S. Brown-Leger, 2004: Collapse and rapid resumption of Atlantic meridional circulation linked to deglacial climate changes. *Nature,* **428,** 834–837.

Moore, G. W. K., and I. A. Renfrew, 2005: Tip jets and barrier winds: A QuikSCAT climatology of high wind speed events around Greenland. *J. Climate,* **18,** 3713–3725.

Pickart, R. S., 1995: Gulf Stream–generated topographic Rossby Waves. *J. Phys. Oceanogr.,* **25,** 574–586.

——, and W. M. Smethie Jr., 1993: How does the Deep Western Boundary Current cross the Gulf Stream? *J. Phys. Oceanogr.,* **23,** 2602–2616.

——, and ——, 1998: Temporal evolution of the Deep Western Boundary Current where it enters the sub-tropical domain. *Deep-Sea Res.,* **45,** 1053–1083.

——, M. A. Spall, and J. R. N. Lazier, 1997: Mid-depth ventilation in the western boundary current system of the sub-polar gyre. *Deep-Sea Res. I,* **44,** 1025–1054.

——, D. J. Torres, and R. A. Clarke, 2002: Hydrography of the Labrador Sea during active convection. *J. Phys. Oceanogr.,* **32,** 428–457.

——, M. A. Spall, M. H. Ribergaard, G. W. K. Moore, and R. F. Milliff, 2003a: Deep convection in the Irminger Sea forced by the Greenland tip jet. *Nature,* **424,** 152–156.

——, F. Straneo, and G. W. K. Moore, 2003b: Is Labrador Sea Water formed in the Irminger Basin? *Deep-Sea Res. I,* **50,** 23–52.

Prater, M. D., 2002: Eddies in the Labrador Sea as observed by profiling RAFOS floats and remote sensing. *J. Phys. Oceanogr.,* **32,** 411–427.

Rahmstorf, S., 1997: Risk of sea-change in the Atlantic. *Nature,* **388,** 825–826.

Reid, J. L., 1994: On the total geostrophic circulation of the North Atlantic Ocean: Flow patterns, tracers, and transports. *Prog. Oceanogr.,* **33,** 1–92.

Renfrew, I. A., G. W. K. Moore, P. S. Guest, and K. Bumke, 2002: A comparison of surface layer and surface turbulent flux observations over the Labrador Sea with ECMWF analyses and NCEP reanalyses. *J. Phys. Oceanogr.,* **32,** 383–400.

Rhein, M., and Coauthors, 2002: Labrador Sea water: Pathways, CFC-inventory, and formation rates. *J. Phys. Oceanogr.,* **32,** 648–665.

Ross, C. K., 1992: Moored current meter measurements across Davis Strait. NAFO SCR Doc. 92/70, 8 pp.

Schmitz, W. J., and M. S. McCartney, 1993: On the North Atlantic circulation. *Rev. Geophys.,* **31,** 29–49.

Smethie, W. M., Jr., and R. A. Fine, 2001: Rates of North Atlantic deep water formation calculated from chlorofluorocarbon inventories. *Deep-Sea Res. I,* **48,** 189–215.

Spall, M. A., 2003: On the thermohaline circulation in flat bottom marginal seas. *J. Mar. Res.,* **61,** 1–25.

——, 2004: Boundary currents and watermass transformation in marginal seas. *J. Phys. Oceanogr.,* **34,** 1197–1213.

——, and R. S. Pickart, 2001: Where does dense water sink? A subpolar gyre example. *J. Phys. Oceanogr.,* **31,** 810–826.

Speer, K. G., H.-J. Isemer, and A. Biastoch, 1995: Water mass formation from revised COADS data. *J. Phys. Oceanogr.,* **25,** 2444–2457.

Stocker, T. F., and A. Schmittner, 1997: Influence of CO_2 emission rates on the stability of the thermohaline circulation. *Nature,* **388,** 862–865.

Straneo, F., 2006: On the connection between dense water formation, overturning, and poleward heat transport in a convective basin. *J. Phys. Oceanogr.,* **36,** 606–628.

Swift, J. H., 1984: The circulation of the Denmark Strait and Iceland-Scotland overflow waters in the North Atlantic. *Deep-Sea Res.,* **31,** 1339–1355.

Talley, L. D., 2003: Shallow, intermediate, and deep overturning components of the global heat budget. *J. Phys. Oceanogr.,* **33,** 530–560.

——, J. L. Reid, and P. E. Robbins, 2003: Data-based meridional overturning streamfunctions for the global ocean. *J. Climate,* **16,** 3213–3226.

Våge, K., R. S. Pickart, G. W. K. Moore, and M. H. Ribergaard, 2007: Winter mixed-layer development in the central Irminger Sea: The effect of strong intermittent wind events. *J. Phys. Oceanogr.,* in press.

Worthington, L. V., 1976: *On the North Atlantic Circulation.* Vol. 6, *The Johns Hopkins Oceanographic Studies,* The Johns Hopkins University Press, 110 pp.

Wright, W. R., 1972: Northern sources of energy for the deep Atlantic. *Deep-Sea Res.,* **19,** 865–877.